**Smart Structures and Systems**, *Vol. 31*, *No. 1* (*2023*) *89-100*
https://doi.org/10.12989/sss.2023.31.1.089


# Parametric study of a new tuned mass damper with pre-strained SMA helical springs for vibration reduction

Hongwang Lv and Bin Huang*

*School of Civil Engineering and Architecture*, *Wuhan University of Technology*, *122 Luoshi Road*, *Hongshan District*, *Wuhan*, *430070*, *China*

(*Received June 20*, *2022*, *Revised September 1*, *2022*, *Accepted September 15*, *2022*)

**Abstract.** This paper conducts a parametric study of a new tuned mass damper with pre-strained superelastic SMA helical springs (SMAS-TMD) on the vibration reduction effect. First, a force-displacement relation model of superelastic SMA helical spring is presented based on the multilinear constitutive model of SMA material, and the tension tests of the six SMA springs fabricated are implemented to validate the mechanical model. Then, a dynamic model of a single floor steel frame with the SMAS-TMD damper is set up to simulate the seismic responses of the frame, which are testified by the shaking table tests. The wire diameter, initial coil diameter, number of coils and pre-strain length of SMA springs are extracted to investigate their influences on the seismic response reduction of the frame. The numerical and experimental results show that, under different earthquakes, when the wire diameter, initial coil diameter and number of coils are set to the appropriate values so that the initial elastic stiffness of the SMA spring is between 0.37 and 0.58 times of classic TMD stiffness, the maximum reduction ratios of the proposed damper can reach 40% as the mass ratio is 2.34%. Meanwhile, when the pre-strain length of SMA spring is in a suitable range, the SMAS-TMD damper can also achieve very good vibration reduction performance. The vibration reduction performance of the SMAS-TMD damper is generally equal to or better than that of the classic optimal TMD, and the proposed damper effectively suppresses the detuning phenomena that often occurs in the classic TMD.

**Keywords:** parametric study; seismic response control; shaking table test; shape memory alloy (SMA) helical springs; tuned mass damper

## 1. Introduction

Passive control is an effective technology to reduce the vibration response of structure under dynamic loads, such as winds and earthquakes (Housner *et al.* 1997, Soong and Spencer 2002, Wu *et al.* 2018). As a typical passive control device, tuned mass damper (TMD) have been widely used in engineering structures, such as the Taipei 101 tower (Taipei) (Chung *et al.* 2009), Shanghai Center Tower (Shanghai) (Lu and Chen 2011), Bloomberg Tower (New York) and Tokyo Skytree (Tokyo). The TMD has been proven to effectively reduce the dynamic response of structures under wind loads (Bortoluzzi *et al.* 2015). However, the TMD is less effective for suppressing structural dynamic response under seismic excitations due to the detuning effect (Casciati and Giuliano 2009, Wong and Harris 2012, Yang and Li 2017). In addition, the viscous damper in TMD implies oil leakage problem in practical engineering, which might dramatically decrease the performance of TMD. To improve the performance of traditional TMD, various new vibration control devices are proposed, such as magnetorheological (MR) TMD (Weber 2014, Weber and Maślanka 2014), eddy current TMD (Bae *et al.* 2012, Chen *et al.* 2017), particle TMD (Liu *et al.* 2020, Lu *et al.* 2018), pounding TMD (Wang *et al.* 2021, Zhang *et al.* 2013) and friction TMD (Carmona *et al.* 2017, Jiang *et al.* 2019).

In the recent two decades, superelastic shape memory alloy (SMA) material has increasing applications in earthquake engineering due to its good corrosion resistance, fatigue resistance, energy dissipating ability and re-centering ability (Casciati 2019, Casciati *et al.* 2009, Li *et al.* 2018, Ozbulut *et al.* 2011, Qian *et al.* 2016, Qiu and Zhu 2017, Song *et al.* 2006, Zhou *et al.* 2018). Furthermore, as an important form of SMA, the application of SMA helical spring in structural vibration control has attracted the attention of many researchers. For instance, Speicher *et al.* (2009) designed an SMA helical spring damper and carried out cyclic loading tests, and the test results show that the damper has good self-centering and damping properties. Attanasi and Auricchio (2011) suggested a new type of isolation device by superelastic SMA helical springs, and it was found that this new isolation device had a good control effect on structural vibrations. Huang *et al.* (2014, 2018) developed novel passive isolation and brace systems based on superelastic SMA helical springs, and the experimental and numerical results showed that the systems had a good energy dissipation capacity. Subsequently, Ding *et al.* (2020) numerically and experimentally studied the influence of two parameters, the ratio of spring diameter to the wire diameter and the pre-strain length, on the vibration reduction performance of SMA helical spring braces. Recently, researchers (Mishra *et al.* 2013, Tian *et al.* 2020) proposed an improved TMD by using superelastic SMA

*Corresponding author, Ph.D., Professor,
E-mail: binhuang@whut.edu.cn



ISSN: 1738-1584 (Print), 1738-1991 (Online)

helical springs, and demonstrated the good control effect of the TMD with SMA springs by numerical simulation. However, it is pointed out in the reference (Tian *et al.* 2020) that the energy dissipation capacity of SMA spring is limited due to the existence of the elastic stage of the force-displacement relationship of SMA helical spring, and the detuning effect of this improved TMD is observed sometimes. Lv (2019) proposed a new tuned mass damper with pre-strained superelastic SMA helical springs, referred to as SMAS-TMD. The pre-strained SMA springs in the SMAS-TMD damper can dissipate more energy than the SMA springs with no pre-strain. And the experimental and numerical results showed that SMAS-TMD has good vibration reduction performance and robustness under seismic excitation. Additionally, it is of great significance to study the fatigue performance of SMA components in practical applications. Several researchers have conducted a number of important studies in this area (Carreras *et al*. 2011, Fang *et al*. 2021, Hashemi *et al*. 2019, Sedlák *et al*. 2014, Sherif and Ozbulut 2018). In this study, the duration of earthquake is usually short, and the fatigue effect on the performance of SMA helical spring is not obvious. Therefore, the fatigue problem of SMA helical spring is not considered in this paper.

In order to further investigate the vibration reduction performance of the SMAS-TMD damper, this paper studies the influence of four main design parameters of SMA spring on the seismic response reduction of the frame. A force-displacement relation model of superelastic SMA helical springs is proposed by using the multilinear constitutive model of SMA material, and the model is verified through the tension tests. Then, a simulation model of a single floor steel frame with the SMAS-TMD damper is established and verified by the shaking table tests. And four main parameters of SMA springs, including the wire diameter, initial coil diameter, number of coils and pre-strain length, are selected to investigate their influences on the seismic response reduction of the SMAS-TMD damper. And the numerical and experimental results show that, under different earthquakes, when the four main parameters of SMA spring are located in a suitable range, the maximum reduction ratios of the proposed damper can be reached. And in these cases, the vibration reduction performance of the SMAS-TMD damper is compared with that of the classic optimal TMD.

## 2. Modeling of superelastic SMA helical spring

### *2.1 Multilinear constitutive model of shape memory alloy*

In this section, a multilinear model about normal stress-strain relation is used to illustrate the mechanical property of SMA material (Motahari and Ghassemieh 2007), which is shown in Fig. 1. This model can avoid solving a number of nonlinear thermodynamic equations and is applicable for the civil engineering field.

In Fig. 1, the multiple linear segment O-T-P-Q-R-S-T-O means a major loop of normal stress-strain relation, and the

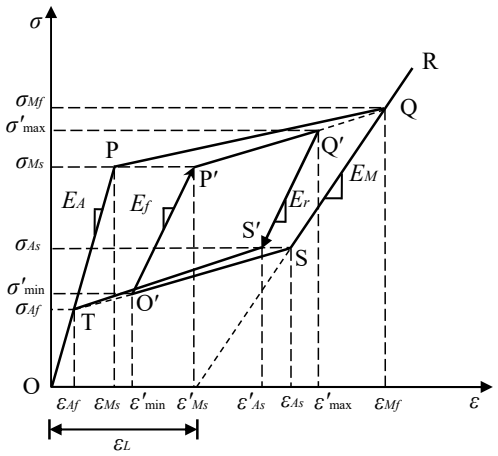


Fig. 1 Normal stress-strain relationship model of SMA material

paths of the major loop are illustrated as follows:

Paths O-P and T-O:

$$\sigma = E_A \varepsilon \tag{1}$$

Path P-Q:

$$\sigma = \sigma_{Ms} + \frac{\sigma_{Mf} - \sigma_{Ms}}{\varepsilon_{Mf} - \varepsilon_{Ms}}(\varepsilon - \varepsilon_{Ms}) \tag{2}$$

Paths Q-R and R-S:

$$\sigma = \sigma_{Mf} + E_M(\varepsilon - \varepsilon_{Mf}) \tag{3}$$

Path S-T:

$$\sigma = \sigma_{As} + \frac{\sigma_{Af} - \sigma_{As}}{\varepsilon_{Af} - \varepsilon_{As}}(\varepsilon - \varepsilon_{As}) \tag{4}$$

where $E_A$ and $E_M$ are Young's modulus of austenite and martensite, respectively. $\sigma_{Ms}$ and $\sigma_{Mf}$ are the starting and final stresses of the martensitic transformation, respectively. $\sigma_{As}$ and $\sigma_{Af}$ are the starting and final stresses of the austenitic transformation, respectively. $\varepsilon_{Ms}$ and $\varepsilon_{Mf}$ are the starting and final strains of the martensitic transformation, respectively, where $\varepsilon_{Ms} = \frac{\sigma_{Ms}}{E_A}$ and $\varepsilon_{Mf} = \varepsilon_L + \frac{\sigma_{Mf}}{E_M}$. $\varepsilon_{As}$ and $\varepsilon_{Af}$ are the starting and final strains of the austenitic transformation, respectively, where $\varepsilon_{As} = \varepsilon_L + \frac{\sigma_{As}}{E_M}$, and $\varepsilon_{Af} = \frac{\sigma_{Af}}{E_A}$. $\varepsilon_L$ is maximum residual strain.

As shown in Fig. 1, when an incomplete phase transformation occurs in SMA material, the stress-strain relationship model of subloop can be depicted by the curve O′-P′-Q′-S′-T. The elastic modulus of the incomplete phase on Path O′-P′ or Q′-S′ differs from that of austenite and martensite, and is a function with respect to martensite volume fraction, which is written as

$$E_i = \frac{E_M E_A}{\xi(E_A - E_M) + E_M}(i = f, r) \tag{5}$$

where $E_f$ and $E_r$ are the elastic moduli of SMA on the Path

O′-P′ and Path Q′-S′, respectively. $\xi$ indicates the martensite volume fraction. $\xi$ is equal to $\frac{(\varepsilon'_{\min}-\varepsilon_{Af})}{(\varepsilon_{As}-\varepsilon_{Af})}$ for the Path O′-P′, and is $\frac{(\varepsilon'_{\max}-\varepsilon_{Ms})}{(\varepsilon_{Mf}-\varepsilon_{Ms})}$ for the Path Q′-S′. $\varepsilon'_{\max}$ and $\varepsilon'_{\min}$ are the maximum and minimum strains in the subloop, respectively.

Based on the elastic modulus defined by means of Eq. (5), the values of critical strain in the subloop can be determined as follows

$$\varepsilon'_{Ms} = \varepsilon'_{\min} + \frac{\sigma_{Ms} - \sigma'_{\min}}{E_f} \tag{6}$$

$$\varepsilon'_{As} = \varepsilon'_{\max} + \frac{\varepsilon_{As} - \varepsilon'_{\max}}{E_r} \tag{7}$$

where $\varepsilon'_{Ms}$ and $\varepsilon'_{As}$ are the strain values at the point P′ and point S′, respectively. The stress-strain relations of diverse paths in the subloop are described in the following.

Path O′-P′:

$$\sigma = \sigma'_{\min} + E_f(\varepsilon - \varepsilon'_{\min}) \tag{8}$$

Path P′-Q′:

$$\sigma = \sigma_{Ms} + \frac{\sigma_{Mf} - \sigma_{Ms}}{\varepsilon_{Mf} - \varepsilon'_{Ms}}(\varepsilon - \varepsilon'_{Ms}) \tag{9}$$

Path Q′-S′:

$$\sigma = \sigma'_{\max} + E_r(\varepsilon - \varepsilon'_{\max}) \tag{10}$$

Path S′-T:

$$\sigma = \sigma_{As} + \frac{\sigma_{Af} - \sigma_{As}}{\varepsilon_{Af} - \varepsilon'_{As}}(\varepsilon - \varepsilon'_{As}) \tag{11}$$

Since the shear stress-strain relationship about the SMA material is experimentally similar to the normal stress-strain relationship, the normal stress and strain in Eqs. (1)-(11) can be replaced by the shear stress and strain accordingly. The related details can be found in the reference (Huang *et al.* 2019).

### *2.2 Force-displacement relationship model of superelastic SMA helical spring*

When a large axial deformation happens in an SMA helical spring, both of bending moment and torsional moment will appear on the cross-section of wire. To describe this mechanical phenomenon, a two-dimensional model (Enemark *et al.* 2016, Huang *et al.* 2019) is used in this paper. As shown in Fig. 2, an axial force $F$ is applied to the SMA helical spring. Assume that for the SMA spring, the coil number is $N$, the initial coil diameter is $D_0$, the wire diameter is $d$, the initial length is $l_0$, and the longitudinal displacement of spring is $u$. The initial pitch angle is $\alpha_0 = arctan\left(\frac{l_0}{(\pi N D_0)}\right)$. The pitch angle of the deformed spring is $\alpha = arcsin\left(\frac{u}{l+sin\,\alpha_0}\right)$, where the total length is $l = \sqrt{l_0^2 + (\pi N D_0)^2}$.

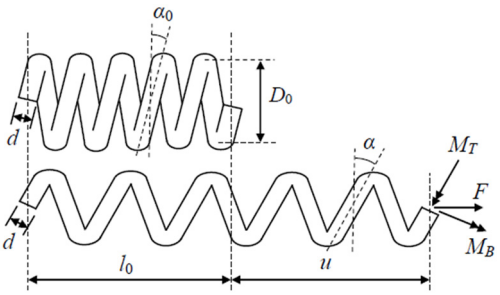


Fig. 2 Schematic of the SMA helical spring

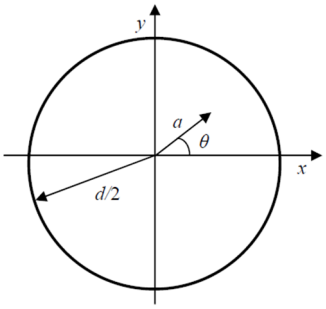


Fig. 3 Schematic diagram of the cross-section of wire

The normal and shear strain distributions on the cross-section of wire can be described as follows

$$\varepsilon(y) = \frac{2y}{D_0} cos\,\alpha_0\,(cos\,\alpha_0 - cos\,\alpha) \tag{12}$$

$$\gamma(a) = \frac{2a}{D_0} cos\,\alpha_0\,(sin\,\alpha - sin\,\alpha_0) \tag{13}$$

where $a$ is the radial coordinate accompanying the angular coordinate $\theta$ and $y$ is the vertical Cartesian coordinate perpendicular to the center axis of the wire, which is plotted in Fig. 3.

Using Eqs. (12) and (13), and considering the multilinear constitutive model of SMA, the distributions of normal and shear stress on the wire cross-section can be achieved. Then the bending moment $M_B$ and the torsional moment $M_T$ on the wire cross-section can be calculated by

$$M_B = \int_0^{\frac{d}{2}} \int_{-\pi}^{\pi} \sigma\big(\varepsilon(\theta,a)\big) a^2\, sin\,\theta\, d\theta da \tag{14}$$

$$M_T = \int_0^{\frac{d}{2}} \int_{-\pi}^{\pi} \tau\big(\gamma(\theta,a)\big)\, a^2 d\theta da \tag{15}$$

where $a$ is the radial coordinate accompanying with the angular coordinate $\theta$, which is plotted in Fig. 3.

As seen in Fig. 2, considering the moment equilibrium related to the torsional moment $M_T$ and bending moment $M_B$ in the spring, the axial force can be written as

$$F = \frac{2\,cos\,\alpha_0}{D_0}(M_T + M_B\,tan\,\alpha) \tag{16}$$

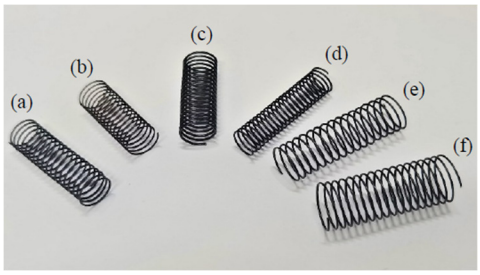


Fig. 4 The SMA spring specimens ((a) SMAS-1; (b) SMAS-2; (c) SMAS-3; (d) SMAS-4; (e) SMAS-5; and (f) SMAS-6)

Table 1 Geometric parameters of specimens

| Specimen | $d$ (mm) | $D_0$ (mm) | $l_0$ (mm) | $N$ |
|---|---|---|---|---|
| SMAS-1 | 0.64 | 11.2 | 16 | 9 |
| SMAS-2 | 0.55 | 11.0 | 18 | 9 |
| SMAS-3 | 0.8 | 11.2 | 17 | 9 |
| SMAS-4 | 0.64 | 9.0 | 14 | 9 |
| SMAS-5 | 0.64 | 12.5 | 18 | 9 |
| SMAS-6 | 0.64 | 14.8 | 19 | 9 |

Following the above procedure, the force-displacement relationship of superelastic SMA helical spring can be determined.

### 2.3 Experimental validation of the proposed mechanical model

To demonstrate the effectiveness of the proposed mechanical model of superelastic SMA helical spring, the Nitinol SMA wires were trained into SMA helical spring specimens in a laboratory. Six trained SMA spring specimens are shown in Fig. 4, and named as SMAS-1, SMAS-2, SMAS-3, SMAS-4, SMAS-5 and SMAS-6, respectively. The geometrical parameters of specimens and the material parameters of SMA are listed in Tables 1 and 2, respectively. Then, a series of the tensile tests of the SMA spring specimens were carried out by a tensile testing machine, as shown in Fig. 5. The comparison of simulated and experimental force-displacement curves are plotted in Fig. 6, which shows the simulation curves agree well with experimental curves. Therefore, the proposed mechanical model of superelastic SMA helical spring can be used in subsequent simulation analysis.

Table 2 Parameters of the SMA material

| $E_A$ (GPa) | $E_M$ (GPa) | $\sigma_{Ms}$ (MPa) | $\sigma_{Mf}$ (MPa) | $\sigma_{As}$ (MPa) | $\sigma_{Af}$ (MPa) | $\varepsilon_L$ |
|---|---|---|---|---|---|---|
| 57 | 30 | 420 | 462 | 271 | 203 | 0.035 |

Fig. 5 Tensile test of SMA spring

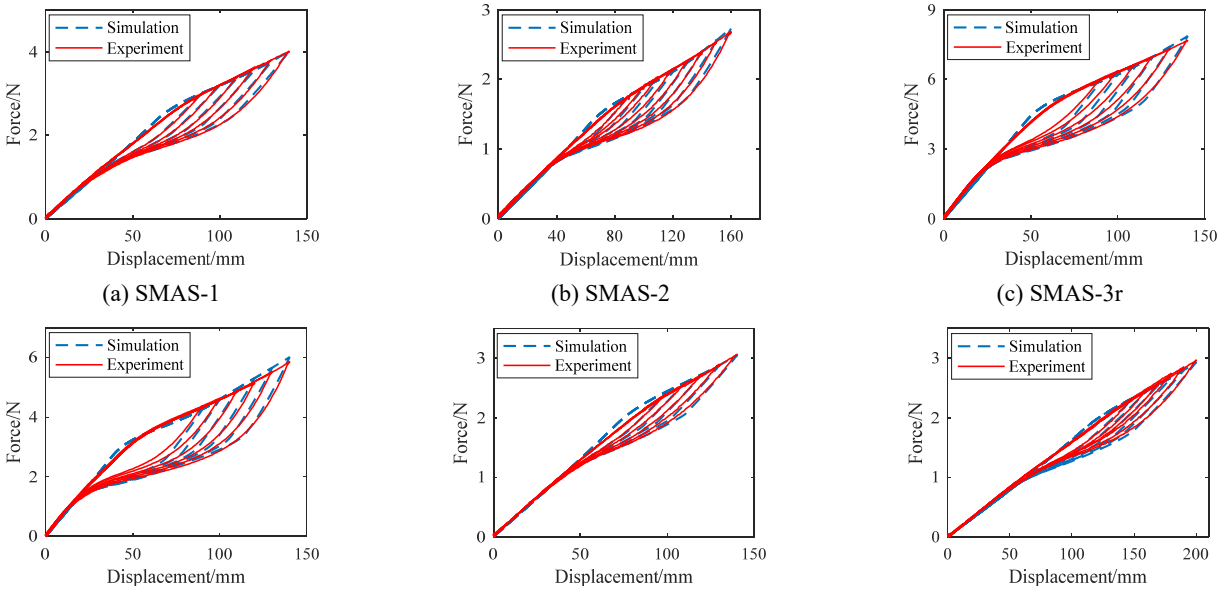


(a) SMAS-1 (b) SMAS-2 (c) SMAS-3r

(d) SMAS-4 (e) SMAS-5 (f) SMAS-6

Fig. 6 The simulated and experimental force-displacement curves of the SMA spring specimens

## 3. Dynamic model of the frame structure with the SMAS-TMD damper

### *3.1 Equation of motion*

The SMAS-TMD mainly consists of two identical pre-strained SMA helical springs and a mass block, a mechanical model of the single floor frame structure with the SMAS-TMD is established, as shown in Fig. 7. The equation of motion of the single floor frame structure with the SMAS-TMD under seismic excitation can be expressed as

$$\begin{cases} m_a\ddot{x}_a + c_a\dot{x}_a + k_a x_a - F_{\text{SMA}} - F_f\, sgn(\dot{x}_b - \dot{x}_a) = -m_a\ddot{x}_g \\ m_b\ddot{x}_b + F_{\text{SMA}} + F_f\, sgn(\dot{x}_b - \dot{x}_a) = -m_b\ddot{x}_g \end{cases} \tag{17}$$

where $m_a$, $k_a$ and $c_a$ are the mass, shear stiffness and damping coefficient of the main structure, respectively. $m_b$ is the mass of the SMAS-TMD. $x_a$ and $x_b$ are the relative displacement of main structure and SMAS-TMD, respectively. $F_f$ is the friction force produced by the motion of the mass block of SMAS-TMD. $F_{\text{SMA}}$ is the resultant force of the SMA helical springs in the SMAS-TMD, which can be calculated by Eq. (16). $\ddot{x}_g$ is the acceleration of the earthquake wave in the horizontal direction. $sgn(\dot{x}_b - \dot{x}_a)$ is a sign function, which can be defined as

$$sgn(\dot{x}_b - \dot{x}_a) = \begin{cases} 1 & (\dot{x}_b - \dot{x}_a > 0) \\ 0 & (\dot{x}_b - \dot{x}_a = 0) \\ -1 & (\dot{x}_b - \dot{x}_a < 0) \end{cases} \tag{18}$$

The Eq. (17) can be solved by using the fourth-order Runge-Kutta method.

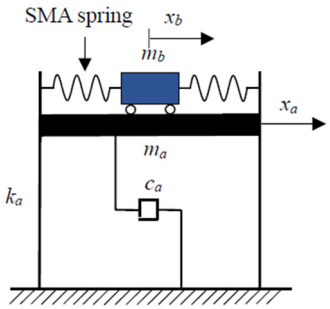


Fig. 7 Mechanical model of the single floor frame structure with the SMAS-TMD

### *3.2 Experimental setup*

A single floor steel frame experimental model was fabricated, as shown in Fig. 8. The length × width × height dimensions of the steel frame are 400 mm × 100 mm × 305 mm. Two accelerometers and two laser displacement sensors were used to measure the dynamic responses of the steel frame.

Based on measurements, the parameters in the Eq. (17) can be obtained. The mass of the main structure is $m_a = 12.118$ kg. The mass of SMAS-TMD is $m_b = 0.283$ kg, and the mass ratio of the SMAS-TMD to the main structure is 2.34%. The friction force is $F_f = 0.06\,N$. The damping ratio $\xi_a = 0.36\%$ and natural frequency $f_a = 2.655$ Hz of the steel frame model are obtained by free vibration test. The shear stiffness of the main structure is $k_a = 3372$ N/m. The damping coefficient of the main structure is $c_a = 1.455\,Ns/m$.

### *3.3 Comparison of the simulated and experimental results*

To verify the effectiveness of the dynamic model of the frame structure with the SMAS-TMD damper under earthquake excitation, a number of shaking table tests are implemented. In the experiments, two cases, which are with and without the SMAS-TMD damper, are investigated. The spring SMAS-1 is selected as the spring component of the SMAS-TMD damper, and the pre-strain length is 100 mm. Four recorded earthquake waves are selected, namely, the San Fernando wave, El Centro wave, Hollister wave and

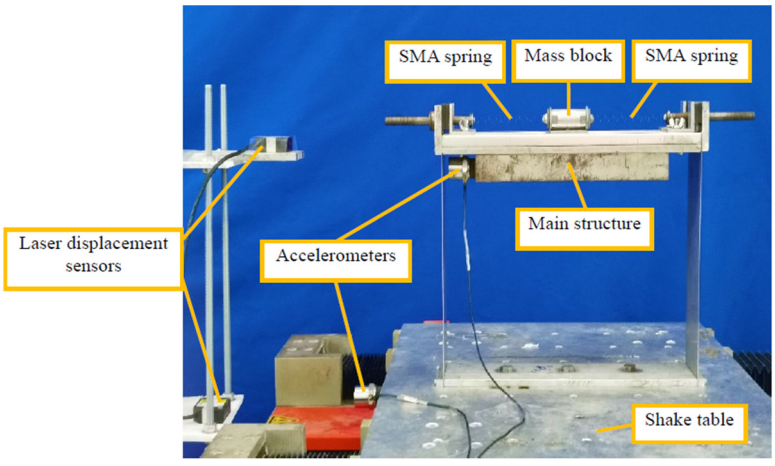


Fig. 8 Shaking table test of the single floor frame structure with the SMAS-TMD

Imperial Valley wave. The peak ground acceleration (PGA) of the four earthquake waves is taken as 0.15 $g$. The acceleration response spectrum of input ground motions are shown in Fig. 9.

As an example, for the San Fernando wave, the comparison of numerical and experimental results of the seismic responses of the main structure are plotted in Fig. 10. Fig. 10 shows that the numerical results agree well with the experimental results for the two cases. Further the relative errors of the simulated peak seismic responses to those from the tests in the two cases are listed in Table 3. From Table 3, it is found that the relative errors of the peak relative displacement and the peak absolute acceleration are within the acceptable range. Therefore, the established dynamic model is available for simulating the dynamic response of the frame structure with the SMAS-TMD under earthquake.

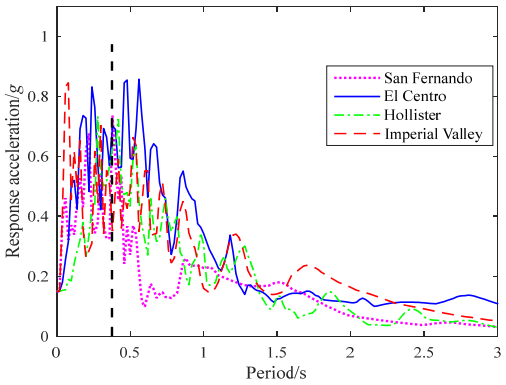


Fig. 9 Acceleration response spectrum of input ground motions

## 4. Parameter study of the SMAS-TMD damper

In the size design of SMA helical spring, the initial coil diameter, wire diameter and number of coils are three important design parameters. According to the reference (Enemark *et al.* 2016), as shown in Fig. 11, the elastic stiffness $k_A$ of the SMA spring can be determined by

$$k_A = \frac{E_A d^4}{16(1+\nu)ND_0^3} \tag{19}$$

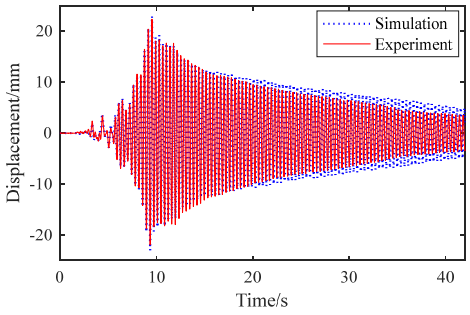


(a) relative displacement (uncontrolled)

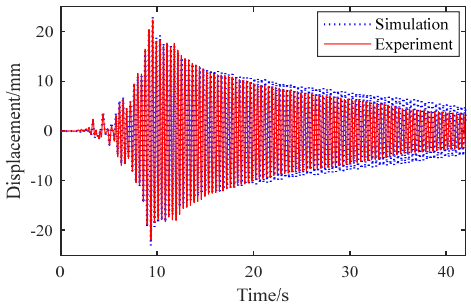


(b) absolute acceleration (uncontrolled)r

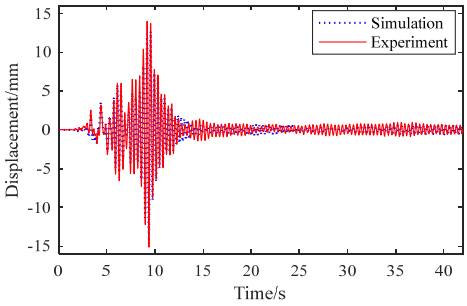


(c) relative displacement (SMAS-TMD)

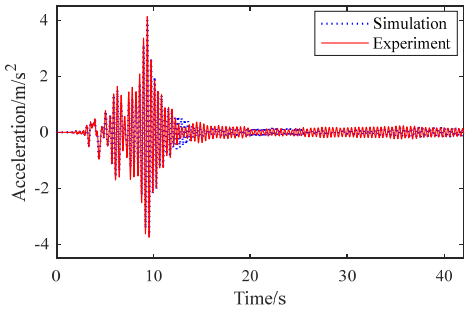


(d) absolute acceleration (SMAS-TMD)

Fig. 10 Numerical and experimental seismic responses for the San Fernando wave

Table 3 Relative errors of the simulated peak seismic responses of the main structure compared to the corresponding test results in the two cases

| Earthquake | Relative errors of peak relative displacement (%) | | Relative errors of peak absolute acceleration (%) | |
|---|---|---|---|---|
| | Uncontrolled | SMAS-TMD | Uncontrolled | SMAS-TMD |
| San Fernando wave | 2.77 | 5.65 | 6.04 | 3.13 |
| El Centro wave | 0.44 | 0.23 | 0.49 | 6.56 |
| Hollister wave | 0.47 | 1.25 | 1.28 | 2.71 |
| Imperial Valley wave | 5.41 | 2.59 | 4.82 | 4.64 |

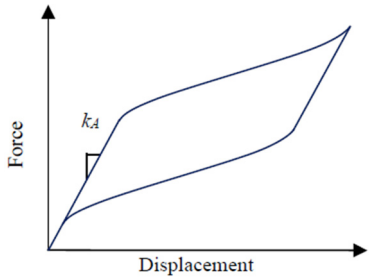


Fig. 11 Schematic of the force-displacement curve of the superelastic SMA helical spring

where $\nu$represents Poisson's ratio and is equal to 0.33 (Huang *et al.* 2019).

If the SMAS-TMD degenerates into a classic linear TMD, the elastic stiffness, $k_T$, of the TMD can be determined by

$$k_T = (2\pi f_a)^2 m_b \tag{20}$$

Considering that two identical SMA springs are arranged on both sides of the mass block of the SMAS-TMD, the elastic stiffness, $k_A$, of the SMA springs is decided as

$$k_A = 0.5k_T \tag{21}$$

However, the above design steps only consider the elastic stage and ignores the phase transformation stage of the SMA spring. Therefore, the initial coil diameter, wire diameter and number of coils need to be redesigned. This section will numerically and experimentally study the effect of the three parameters on the vibration reduction performance of the SMAS-TMD. In addition, the influence of the pre-strain length of SMA spring on the control performance of SMAS-TMD is also studied in this section. Four earthquake waves are selected, which are the same as those shown in Fig. 8. The PGA of the four earthquake waves is taken as 0.15 $g$. The reduction ratio of peak response is defined as follows

### *4.1 Effect of wire diameter*

In the simulation, the wire diameter of SMA spring varies from 0.5 mm to 1 mm. The initial coil diameter, number of coils and pre-stretch length are set to 11.2 mm, 9 and 100 mm, respectively. In the shaking table tests, the specimens SMAS-1, SMAS-2 and SMAS-3 are selected as the spring component of the SMAS-TMD damper, respectively. The reduction ratios of peak responses along with the increase of wire diameter under the four earthquake waves are numerically and experimentally obtained, and are plotted in Fig. 12. It is seen from Fig. 12(a) that the simulated results agree well with the experimental results. The reduction ratio of peak relative displacement first increases and then decreases as the wire diameter increases. About the reduction ratio of peak absolute acceleration, the similar result can be observed from Fig. 12(b). It is also found that when the wire diameter is between 0.61 mm and 0.68 mm, the reduction ratios of peak seismic responses achieve the maximum values under the four earthquake waves. And apart from the Hollister earthquake, the maximum reduction ratios for the other three earthquakes are close to 40%. In addition, according to the Eqs. (19) and (20), the SMA spring elastic stiffness $k_A$ is between $0.37k_T$ and $0.58k_T$, where the wire diameter is between 0.61 mm and 0.68 mm correspondingly.

### *4.2 Effect of initial coil diameter*

In the shaking table tests, the specimens SMAS-1, SMAS-4, SMAS-5 and SMAS-6 are selected as the spring component of the SMAS-TMD, respectively. In the simulation, the initial coil diameter of SMA spring changes from 9 mm to 15 mm. The wire diameter, number of coils, pre-stretch length are set to 0.64 mm, 9 and 100 mm, respectively. Fig. 13 shows that the reduction ratios of peak responses along with the increase of initial coil diameter under the four earthquake waves. From Fig. 13, it is seen that the experimental and simulated results are consistent. It is found from Fig. 13(a) that the reduction ratio of peak

$$\text{Reduction ratio} = \frac{\text{the peak response of the frame} - \text{the peak response of the frame with SMAS} - \text{TMDMD}}{\text{the peak response of the frame}} \times 100\% \tag{22}$$

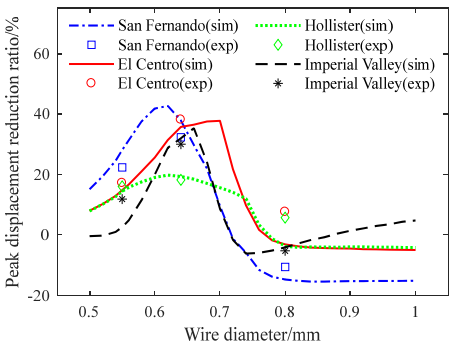


(a) Peak relative displacement

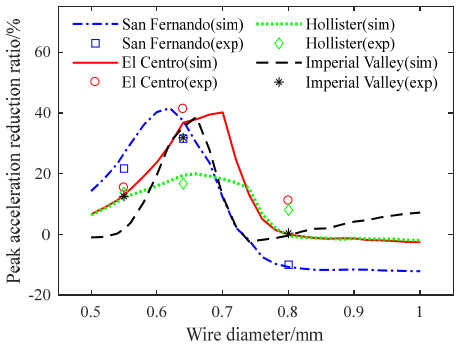


(b) Peak absolute acceleration

Fig. 12 The reduction ratios of peak responses along with the increase of wire diameter

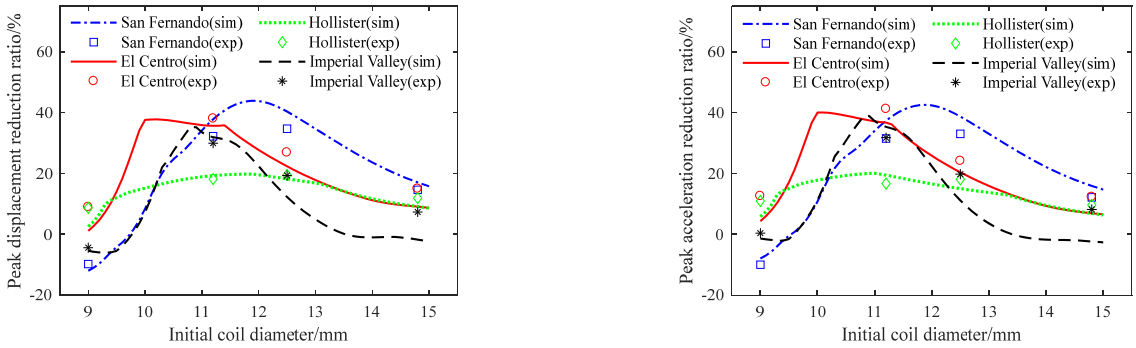


(a) Peak relative displacement (b) Peak absolute acceleration

Fig. 13 The reduction ratios of peak responses along with the increase of initial coil diameter

relative displacement first increases and then decreases as initial coil diameter increases. From Fig. 13(b), it is also found that with the increase of the initial coil diameter, the reduction ratio of peak absolute acceleration has the same trend as the reduction ratio of peak relative displacement. And the vibration reduction performance of the SMAS-TMD damper is satisfactory when the initial coil diameter varies from 10.3 mm to 12 mm, where the SMA spring elastic stiffness $k_A$ is between $0.37k_T$ and $0.58k_T$.

### *4.3 Effect of number of coils*

To study the influence of number of coils on the vibration reduction performance of the SMAS-TMD damper, damper, in the experiments, the number of coils is given as 7, 9, 11 and 13, respectively. The wire diameter, initial coil diameter and pre-strain length of the SMA spring are 0.64 mm, 11.2 mm and 100 mm, respectively. And the number of coils is varied from 7 to 13 in the simulation. Under the four earthquake waves, the reduction ratios of peak responses along with the variation of the number of coils are plotted in Fig. 14. From Fig. 14, it is found that the numerical results are basically consistent with the experimental results. When the number of coils is in the range of 8 to 10, the reduction ratios of the peak responses can reach about 20% to 40% no matter for the peak relative displacement or the peak absolute acceleration. The interesting thing is that at those situations, the SMA spring elastic stiffness $k_A$ is also in the

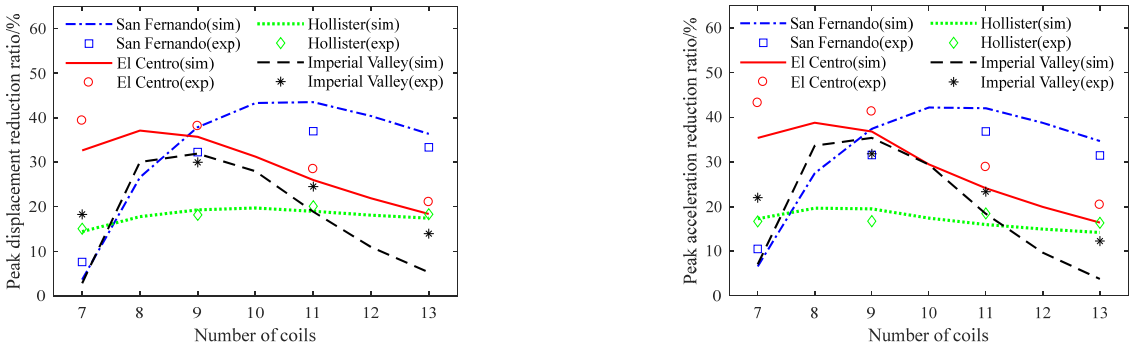


(a) Peak relative displacement (b) Peak absolute acceleration

Fig. 14 The reduction ratios of peak responses along with the increase of number of coils

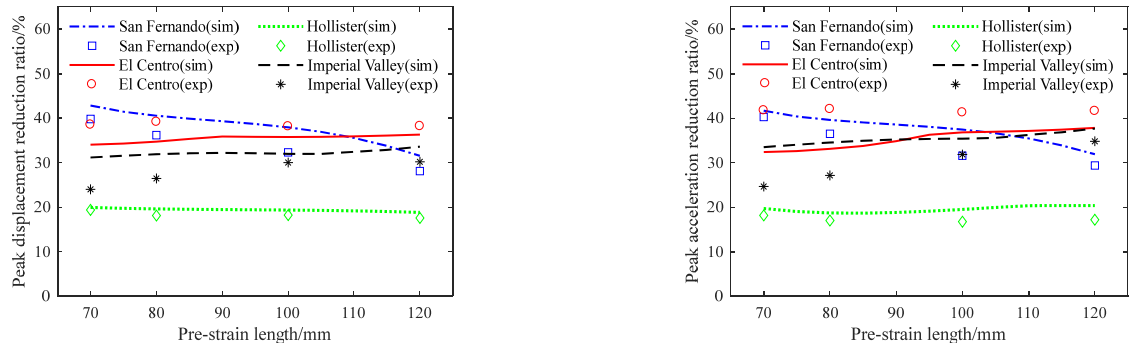


(a) Peak relative displacement (b) Peak absolute acceleration

Fig. 15 The reduction ratios of peak responses along with the increase of pre-strain length

Table 4 Information of 20 recorded earthquake waves

| No. | Earthquake | Station | Year |
|---|---|---|---|
| 1 | Northwest Calif | Ferndale City Hall | 1938 |
| 2 | Imperial Valley | El Centro Terminal Substation Building | 1940 |
| 3 | Hollister | Usgs Station 1028 | 1961 |
| 4 | Parkfield | San Luis Obispo | 1966 |
| 5 | San Fernando | Pacoima Dam (upper left abut) | 1971 |
| 6 | Friuli | Forgaria Cornino | 1976 |
| 7 | Tabas | Dathook | 1978 |
| 8 | Tabas | Sedeh | 1978 |
| 9 | Imperial Valley | Agrarias | 1979 |
| 10 | Coyote Lake | Gilroy Array #4 | 1979 |
| 11 | Loma Prieta | Oakland-Title & Trust | 1989 |
| 12 | Landers | Amboy | 1992 |
| 13 | Northridge | Pacoima Kagel Canyon | 1994 |
| 14 | Kobe | Fukushima | 1995 |
| 15 | Chi-Chi | CHY024 | 1999 |
| 16 | Chi-Chi | ILA039 | 1999 |
| 17 | Duzce | Hava Alani | 1999 |
| 18 | Hector Mine | El Centro Array #10 | 1999 |
| 19 | Gulf of California | El Centro-Meadows Union School | 2001 |
| 20 | El Mayor | El Centro-Meloland Geot. Array | 2010 |

range of $0.37k_T$ to $0.58k_T$.

### *4.4 Effect of pre-strain length*

Due to the limitation of the frame width, the maximum pre-strain length of SMA spring needs to be less than 120 mm in shaking table experiments. The specimen SMAS-1 are used as the spring component of the damper and the pre-strain length is designed as 70 mm, 80 mm, 100 mm and 120 mm, respectively. The wire diameter, initial coil diameter and number of coils of the SMA spring are 0.64 mm, 11.2 mm and 9, respectively. The reduction ratios of peak seismic responses along with the variation of pre-strain length under four earthquake waves are obtained by numerical simulations and experiments, and are plotted in Fig. 15. From Fig. 15, it is found that when the pre-strain length increases from 70 mm to 120 mm, the reduction ratios of peak responses decrease gradually under the San Fernando wave. Under other earthquake waves, the variation of reduction ratio is small. Compared with the initial coil diameter, the wire diameter and the number of coils, the influence of pre-strain length on the reduction ratio is not large. When the pre-strain length varies from 90 mm to 110 mm, the vibration reduction performance of the SMAS-TMD damper is satisfactory under the four earthquake waves.

## 5. Vibration reduction performance of the SMAS-TMD damper with the optimal parameters

This section numerically studies the vibration reduction effect of the proposed SMAS-TMD damper under the earthquakes with the PGA of 0.2 *g*. The frame model in

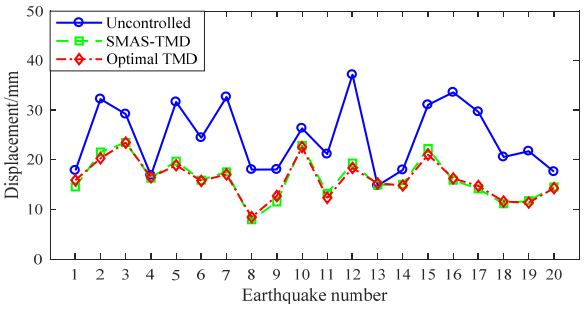


(a) The original frame

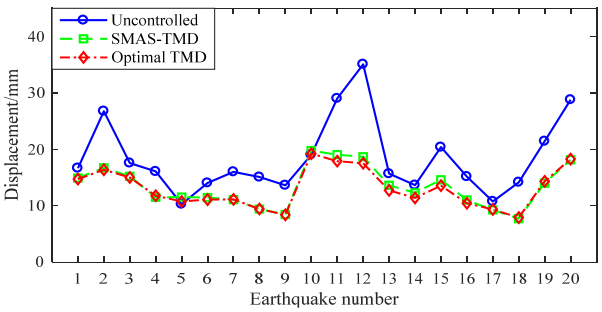


(b) The frame with 15% increased structural frequency

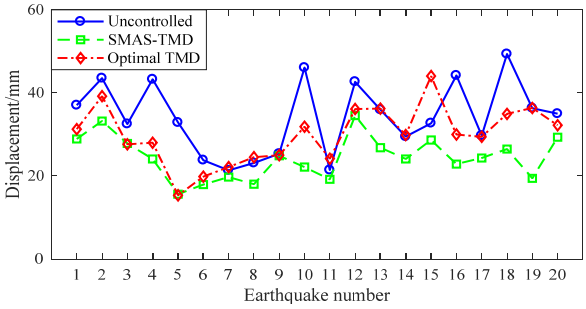


(c) The frame with 15% reduced structural frequency

Fig. 16 Peak relative displacement of the frame under the 20 earthquake waves

Table 5 Average reduction ratios of the peak relative displacement under the 20 earthquake waves

| Structural frequency | Optimal TMD | SMAS-TMD |
|---|---|---|
| 15% increased | 26.46% | 24.48% |
| Original | 32.06% | 32.08% |
| 15% reduced | 10.21% | 26.30% |

Section 3.2 is adopted in the simulation and the mass ratio of the SMAS-TMD is set to 2.34%. According to the above parametric study, the optimal parameters of SMA spring component of the SMAS-TMD damper may take the parameters of the specimen SMAS-1 and the pre-strained length is set to 100 mm. For comparison, the vibration reduction effectiveness of the classic optimal TMD is also discussed. Given that the mass ratio is the same as that of the SMAS-TMD damper, the optimal parameters of the classic TMD are determined by the Den Hartog formulas (Den Hartog 1956), where the optimal tuning ratio and damping ratio of the TMD are 0.9772 and 9.25%, respectively. A total of 20 recorded earthquake waves, as shown in Table 4, are selected for the study.

When the true structural natural frequencies are different from the designed values, the detuning effect often happens for the classic TMD system. So, besides the original status, the situations that the frequency of the original frame increases or reduces 15% are considered here. The average reduction ratios of the peak relative displacement under the 20 earthquake waves are listed in Table 5. The peak relative displacements of the top of the frame are calculated and plotted in Fig. 16. From Table 5 and Figs. 16(a) and (b), it is found that for the original frame and the frame with 15% increase of frequency, the relative displacements with the SMAS-TMD damper are close to that with the optimal TMD. On the other hand, Table 5 and Fig. 16(c) show that if the structural frequency reduces 15%, the displacements of the frame with the SMAS-TMD damper is obviously less than those with the optimal TMD. Also from Fig. 16(c), it is observed that in the case of No. 15 earthquake, the result with the optimal TMD is amplified compared to that without damper, which indicates that the detuning phenomenon occurs. And in this case, the vibration reduction performance of the proposed SMAS-TMD damper is still very good.

## 6. Conclusions

This paper conducts a parametric study of a new SMAS-TMD damper with pre-strained SMA springs for vibration reduction. A force-displacement relation numerical model of SMA helical spring is presented, the effectiveness of which is verified by the tension tests. On that basis, the dynamic numerical model of a single floor frame with the proposed SMAS-TMD damper under earthquake is established and validated by the shaking table tests. Then the influences of four main design parameters of the SMAS-TMD damper, namely, the wire diameter, initial coil diameter, number of coils and pre-strain length on the seismic responses of the frame are investigated.

- The numerical and experimental results demonstrate that when the wire diameter, initial coil diameter and number of coils are set to the appropriate values so that the designed elastic stiffness $k_A$ of the SMA spring is in the range of $0.37k_T$ to $0.58k_T$, the vibration reduction performance of the SMAS-TMD damper is satisfactory. And the maximum reduction ratios of the SMAS-TMD damper can reach 40% as the mass ratio is 2.34%. Under different earthquake waves, when the pre-strain length of the SMA springs varies from 90 mm to 110 mm, the vibration reduction performance of the SMAS-TMD damper is very well.
- The numerical results also show that when the structural frequency decreases by 15%, for the classic optimal TMD, the seismic responses of the frame are amplified compared to those without TMD under some situations, which means that the detuning phenomenon occurs. However, the proposed SMAS-TMD damper can effectively suppress the responses of the frame under 20 recorded earthquakes with the same detuning ratio, which demonstrates the robustness of the proposed SMAS-TMD damper.

## Acknowledgments

The authors would like to acknowledge the financial support from the National Natural Science Foundation of China (Project No. 51578431 and 51978545).

## References

Attanasi, G. and Auricchio, F. (2011), "Innovative superelastic isolation device", *J. Earthq. Eng.*, **15**(S1), 72-89. https://doi.org/10.1080/13632469.2011.562406

Bae, J.S., Hwang, J.H., Roh, J.H. and Kim, J.H. (2012), "Vibration suppression of a cantilever beam using magnetically tuned-mass-damper", *J. Sound Vib.*, **331**(26), 5669-5684. https://doi.org/10.1016/j.jsv.2012.07.020

Bortoluzzi, D., Casciati, S., Elia, L. and Faravelli, L. (2015), "Design of a TMD solution to mitigate wind-induced local vibrations in an existing timber footbridge", *Smart Struct. Syst., Int. J.*, **16**(3), 459-478. https://doi.org/10.12989/sss.2015.16.3.459

Carmona, J.E.C., Avila, S.M. and Doz, G. (2017), "Proposal of a tuned mass damper with friction damping to control excessive floor vibrations", *Eng. Struct.*, **148**, 81-100. https://doi.org/10.1016/j.engstruct.2017.06.022

Carreras, G., Casciati, F., Casciati, S., Isalgue, A., Marzi, A. and Torra, V. (2011), "Fatigue laboratory tests toward the design of SMA portico-braces", *Smart Struct. Syst., Int. J.*, **7**(1), 41-57. https://doi.org/10.12989/sss.2011.7.1.041

Casciati, S. (2019), "SMA-based devices: insight across recent proposals toward civil engineering applications", *Smart Struct. Syst., Int. J.*, **24**(1), 111-125. https://doi.org/10.12989/sss.2019.24.1.111

Casciati, F. and Giuliano, F. (2009), "Performance of multi-TMD in the towers of suspension bridges", *J. Vib. Control*, **15**(6), 821-847. https://doi.org/10.1177/1077546308091455

Casciati, F., Faravelli, L. and Al, S.R. (2009), "An SMA passive device proposed within the highway bridge benchmark", *Struct.*

*Control Health Monit*., **16**(6), 657-667. https://doi.org/10.1002/stc.332

Chen, J.D., Lu, G.T., Li, Y.R., Wang, T., Wang, W.X. and Song, G. (2017), "Experimental study on robustness of an eddy current-tuned mass damper", *Appl. Sci*., **7**(9), 895. https://doi.org/10.3390/app7090895

Chung, L.L., Wu, L.Y., Huang, H.H., Chang, C.H. and Lien, K.H. (2009), "Optimal design theories of tuned mass dampers with nonlinear viscous damping", *Earthq. Eng. Eng. Vib*., **8**(4), 547-560. https://doi.org/10.1007/s11803-009-9115-3

Den Hartog, J.P. (1956), *Mechanical Vibrations*, McGraw-Hill, New York, NY, USA.

Ding, J.C., Huang, B., Lv, H.W. and Wan, H.X. (2020), "Parametric study of SMA helical spring braces for the seismic resistance of a frame structure", *Smart Struct. Syst.*, *Int. J*., **25**(3), 311-322. https://doi.org/10.12989/sss.2020.25.3.311

Enemark, S., Santos, I.F. and Savi, M.A. (2016), "Modelling, characterisation and uncertainties of stabilised pseudoelastic shape memory alloy helical springs", *J. Intell. Mater. Syst. Struct*., **27**(20), 2721-2743. https://doi.org/10.1177/1045389X16635845

Fang, C., Wang, W., Ji Y.Z. and Yam, M.C.H. (2021), "Superior low-cycle fatigue performance of iron-based SMA for seismic damping application", *J. Constr. Steel Res*., **184**, 106817. https://doi.org/10.1016/j.jcsr.2021.106817

Hashemi, Y.M., Kadkhodaei, M. and Mohammadzadeh, M.R. (2019), "Fatigue Analysis of Shape Memory Alloy Helical Springs", *Int. J. Mech. Sci*., **161-162**, 105059. https://doi.org/10.1016/j.ijmecsci.2019.105059

Housner, G.W., Bergman, L.A., Caughey, T.K., Chassiakos, A.G., Claus, R.O., Masri, S.F., Skelton, R.E., Soong, T.T., Spencer, B.F. and Yao, J.T.P. (1997), "Structural control: Past, present, and future", *J. Eng. Mech*., **123**(9), 897-971. https://doi.org/10.1061/(ASCE)0733-9399(1997)123:9(897)

Huang, B., Zhang, H.Y., Wang, H. and Song, G. (2014), "Passive base isolation with superelastic nitinol SMA helical springs", *Smart Mater. Struct*., **23**(6), 065009. https://doi.org/10.1088/0964-1726/23/6/065009

Huang, B., Lao, Y.M., Chen, J.M. and Song, Y. (2018), "Dynamic response analysis of a frame structure with superelastic nitinol SMA helical spring braces for vibration reduction", *J. Aerosp. Eng*., **31**(6), 04018096. https://doi.org/10.1061/(ASCE)AS.1943-5525.0000923

Huang, B., Lv, H.W. and Song, Y. (2019), "Numerical simulation and experimental study of a simplified force-displacement relationship in superelastic SMA helical springs", *Sensors*, **19**(1), 50. https://doi.org/10.3390/s19010050

Jiang, J.W., Ho, S.C.M., Markle, N.J., Wang, N. and Song, G. (2019), "Design and control performance of a frictional tuned mass damper with bearing–shaft assemblies", *J. Vib. Control*, **25**(12), 1812-1822. https://doi.org/10.1177/1077546319832429

Li, H.N., Liu, M.M. and Fu, X. (2018), "An innovative re-centering SMA-lead damper and its application to steel frame structures", *Smart Mater. Struct*., **27**(7), 075029. https://doi.org/10.1088/1361-665X/aac28f

Liu, S.T., Lu, Z., Li, P.Z., Zhang, W.Y. and Taciroglu, E. (2020), "Effectiveness of particle tuned mass damper devices for pile-supported multi-story frames under seismic excitations", *Struct. Control Health Monit*., **27**(11), e2627. https://doi.org/10.1002/stc.2627

Lu, X.L. and Chen, J.R. (2011), "Mitigation of wind-induced response of Shanghai Center Tower by tuned mass damper", *Struct. Des. Tall Spec. Build*., **20**(4), 435-452. https://doi.org/10.1002/tal.659

Lu, Z., Li, K. and Zhou, Y. (2018), "Comparative studies on structures with a tuned mass damper and a particle damper", *J. Aerosp. Eng*., **31**(6), 04018090. https://doi.org/10.1061/(ASCE)AS.1943-5525.0000878

Lv, H.W. (2019), "Experimental study and theoretical analysis of SMAS-TMD system in vibration control of structure", M.S. Dissertation; Wuhan University of Technology, Wuhan, China.

Mishra, S.K., Gur, S. and Chakraborty, S. (2013), "An improved tuned mass damper (SMA-TMD) assisted by a shape memory alloy spring", *Smart Mater. Struct*., **22**(9), 095016. https://doi.org/10.1088/0964-1726/22/9/095016

Motahari, S.A. and Ghassemieh, M. (2007), "Multilinear one-dimensional shape memory material model for use in structural engineering applications", *Eng. Struct*., **29**(6), 904-913. https://doi.org/10.1016/j.engstruct.2006.06.007

Ozbulut, O.E., Hurlebaus, S. and Desroches, R. (2011), "Seismic response control using shape memory alloys: a review", *J. Intell. Mater. Syst. Struct*., **22**(14), 1531-1549. https://doi.org/10.1177/1045389X11411220

Qian, H., Li, H.N. and Song, G. (2016), "Experimental investigations of building structure with a superelastic shape memory alloy friction damper subject to seismic loads", *Smart Mater. Struct*., **25**(12), 125026. https://doi.org/10.1088/0964-1726/25/12/125026

Qiu, C.X. and Zhu, S.Y. (2017), "Shake table test and numerical study of self-centering steel frame with SMA braces", *Earthq. Eng. Struct. Dyn*., **46**(1), 117-137. https://doi.org/10.1002/eqe.2777

Sedlák, P., Frost, M., Kruisová, A., Hiřmanová, K., Heller, L. and Šittner, P. (2014), "Simulations of Mechanical Response of Superelastic NiTi Helical Spring and its Relation to Fatigue Resistance", *J. Mater. Eng. Perform*., **23**(7), 2591-2598. https://doi.org/10.1007/s11665-014-0906-y

Sherif, M.M. and Ozbulut, O.E. (2018), "Tensile and superelastic fatigue characterization of NiTi shape memory cables", *Smart Mater. Struct*., **27**(1), 015007. https://doi.org/10.1088/1361-665X/aa9819

Song, G., Ma, N. and Li. H.N. (2006), "Applications of shape memory alloys in civil structures", *Eng. Struct*., **28**(9), 1266-1274. https://doi.org/10.1016/j.engstruct.2005.12.010

Soong, T.T. and Spencer, B.F. (2002), "Supplemental energy dissipation: state-of-the-art and state-of-the-practice", *Eng. Struct*., **24**(3), 243-259. https://doi.org/10.1016/S0141-0296(01)00092-X

Speicher, M.S., Hodgson, D.E., Desroches, R. and Leon, R. (2009), "Shape memory alloy tension/compression device for seismic retrofit of buildings", *J. Mater. Eng. Perform*., **18**(5-6), 746-753. https://doi.org/10.1007/s11665-009-9433-7

Tian, L., Zhou, M.Y., Qiu, C.X., Pan, H.Y. and Rong, K.J. (2020), "Seismic response control of transmission tower-line system using SMA-based TMD", *Struct. Eng. Mech.*, *Int. J*., **74**(1), 129-143. https://doi.org/10.12989/sem.2020.74.1.129

Wang, W.X., Yang, Z.L., Hua, X.G., Chen, Z.Q., Wang, X.Y. and Song, G. (2021), "Evaluation of a pendulum pounding tuned mass damper for seismic control of structures", *Eng. Struct*., **228**, 111554. https://doi.org/10.1016/j.engstruct.2020.111554

Weber, F. (2014), "Semi-active vibration absorber based on real-time controlled MR damper", *Mech. Syst. Signal Proc*., **46**(3), 272-288. https://doi.org/10.1016/j.ymssp.2014.01.017

Weber, F. and Maślanka, M. (2014), "Precise stiffness and damping emulation with MR dampers and its application to semi-active tuned mass dampers of Wolgograd Bridge", *Smart Mater. Struct*., **23**(1), 015019. https://doi.org/10.1088/0964-1726/23/1/015019

Wong, K.K.F. and Harris, J.L. (2012), "Seismic damage and fragility analysis of structures with tuned mass dampers based on plastic energy", *Struct. Des. Tall Spec. Build*., **21**(4), 296-310. https://doi.org/10.1002/tal.604

Wu, Q.Y., Dai, J.Z. and Zhu, H.P. (2018), "Optimum design of passive control devices for reducing the seismic response of

twin-tower-connected structures", *J. Earthq. Eng*., **22**(5), 826-860. https://doi.org/10.1080/13632469.2016.1264332

Yang, Y.Z. and Li, C.X. (2017), "Performance of tuned tandem mass dampers for structures under the ground acceleration", *Struct. Control Health Monit*., **24**(10), e1974. https://doi.org/10.1002/stc.1974

Zhang, P., Song, G., Li, H.N. and Lin, Y.X. (2013), "Seismic Control of Power Transmission Tower Using Pounding TMD", *J. Eng. Mech*., **139**(10), 1395-1406. https://doi.org/10.1061/(ASCE)EM.1943-7889.0000576

Zhou, P., Liu, M., Li, H. and Song, G. (2018), "Experimental investigations on seismic control of cable-stayed bridges using shape memory alloy self-centering dampers", *Struct. Control Health Monit*., **25**(7), e2180. https://doi.org/10.1002/stc.2180

*FC*